Applied Thermal Engineering 190 (2021) 116726

Contents lists available at ScienceDirect

Applied Thermal Engineering

journal homepage: www.elsevier.com/locate/apthermeng

# Transformation heat transfer and thermo-hydrodynamic cloaks for creeping flows: Manipulating heat fluxes and fluid flows simultaneously

Bin Wang [a,b], Tien-Mo Shih [c], Jiping Huang [a]

[a] Department of Physics, State Key Laboratory of Surface Physics, and Key Laboratory of Micro and Nano Photonic Structures (MOE), Fudan University, Shanghai 200438, China
[b] School of Mechanical and Power Engineering, East China University of Science and Technology, Shanghai 200237, China
[c] Department of Mechanical Engineering, University of California, Berkeley, CA 94720, USA

ARTICLE INFO

*Keywords:*
Transformation heat transfer
Thermo-hydrodynamic cloaks
Metamaterials
Creeping flows
COMSOL

ABSTRACT

Although the subject of thermal cloaking has attracted extensive academic attention, most pioneering studies have so far focused on thermal conduction systems or thermal convection in the porous media, which prevents the object from moving. Here, we have discovered that Stokes equations and the energy transport equation do abide by the coordinate-transformation invariant theory if the former is replaced with the pressure Laplace equation. This discovery enables us to rightfully take advantage of the merit of this theory and to analytically design metamaterial thermo-hydrodynamic cloaks. More importantly, since our designed cloaks depend on the viscosity and the thermal conductivity of background flows as well as geometries of cloaks only, but not on boundary conditions of background flows, they can be continuously utilized when objects travel in the media under realistic flow conditions. Besides, we also suggest experimental demonstrations to show the feasibility of our design. Finally, it is our hope that numerical data obtained in the proposed study can (1) facilitate the realization of lab experiments as well as help them identify characteristic flow and thermal parameters, and (2) serve as a stepping stone to further explore other thermo-hydrodynamic metamaterial devices.

## 1. Introduction

Design of metamaterials has been extensively proposed in various fields, such as optics [1–4], electromagnetics [5–9], acoustics [7,10,11], liquid waves [12–14], and quantum mechanical matter waves [15,16].

Particularly, thermal metamaterials have been theoretically designed or experimentally realized and have served as instrumental tools to manipulate heat transfer or to harness energy [17–21], such as thermal cloaks [22–32], thermal camouflages [33–35], thermal concentrators [24,25], thermal rotators [25], macroscopic thermal diodes [28,36], and thermal transparency [37,38], and so forth. More comprehensive investigations of thermal metamaterials can be found in reviews [39–41] and the book [42]. Up to today, most pioneering researchers have primarily focused on controlling heat conduction. Although the convection in fluid flows often behaves dominantly in heat transfer, it has been rarely explored due to its nonlinearity that seems to complicate problems.

Facing this challenge, numerous investigations [43–46] have been dedicated to hydrodynamic metamaterials by manipulating the permeability, such as creeping flows in porous media based on Darcy's law and coordinate-transformation invariant theory [45,46]. Based on these investigations, several thermal cloaks combining thermal conduction and thermal convection in porous media are fabricated [47–49]. Nevertheless, in their studies, the object remains motionless in the porous media, suggesting that applications of cloaks are still stationary.

Beyond these creeping flows in porous media, recently, hydrodynamic metamaterial cloaks by utilizing the hydrodynamic transformation theory [50] and the scattering cancel method [51] in non-porous media for Stokes flows have been investigated. In these investigations [50,51], however, continuum equations that govern thermal convection and conduction have not been solved.

In the proposed study, to overcome drawbacks of previous investigations mentioned above, we have extended "transformation thermal conduction" to "transformation heat transfer", as well as theoretically and numerically demonstrated thermo-hydrodynamic cloaks based on the latter, which can manipulate the coupling of thermal flows and convective flows for non-porous media creeping flows. Treating and controlling both dynamic viscosity and thermal conductivity of our cloaks as tensors, we can accomplish both process of thermal cloaking and hydrodynamic cloaking simultaneously.

*E-mail addresses:* bwang@ecust.edu.cn (B. Wang), tienmoshih@gmail.com (T.-M. Shih), jphuang@fudan.edu.cn (J. Huang).

https://doi.org/10.1016/j.applthermaleng.2021.116726
Received 8 September 2020; Received in revised form 4 February 2021; Accepted 9 February 2021
Available online 28 February 2021
1359-4311/

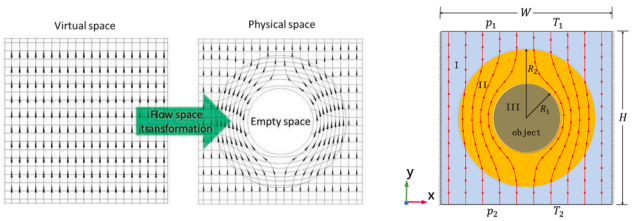


(a) (b)

**Fig. 1.** Schematic models of (a) the coordinate transformation and (b) the thermo-hydrodynamic cloak, where three regimes (I, II, III) represent background, cloak, and object, respectively.

## 2. Transformation heat-transfer equations and analytical cloak parameters

Continuum equations that govern continuity, momentum transport, and energy transports for steady-state incompressible creeping flows without body forces are written as

$$\nabla\cdot\boldsymbol{u} = 0, \tag{1}$$

$$\nabla p = \mu\nabla^2\boldsymbol{u}, \tag{2}$$

$$\rho c_p\nabla\cdot(\boldsymbol{u}T) = \nabla\cdot(k\nabla T). \tag{3}$$

where $u,p$ and $T$ are velocity vector, pressure and temperature, respectively. And symbols $\rho,c_p,\mu$, and $k$ denote density, heat capacity, dynamic viscosity, and thermal conductivity, respectively. With aid of Eq. (1), Eq. (2) can be transformed into Appendix A.1

$$\nabla\cdot\left(\mu^{-1}\nabla p\right) = 0. \tag{4}$$

We can prove that Eqs. (1, 4), (3) remain invariant under the coordinate transformation Appendix A.1. Introducing a Jacobian-transformation matrix ($J$) such that Eqs. (1, 4, 3) from virtual space $\boldsymbol{x}(x, y, z)$ to physical space $\boldsymbol{x}'(x', y', z')$ leads to

$$\nabla'\cdot\boldsymbol{u}' = 0, \tag{5}$$

$$\nabla'\cdot\left(\mu'^{-1}\nabla' p'\right) = 0, \tag{6}$$

$$\rho c_p\nabla'\cdot(\boldsymbol{u}'T') = \nabla'\cdot(k'\nabla'T'), \tag{7}$$

where $\boldsymbol{u}' = J\boldsymbol{u}/\det(J)$,

$$\mu' = \det(J)\cdot J^{-1}\mu J^{-\mathrm{T}}, \tag{8}$$

and

$$k' = JkJ^{\mathrm{T}}/\det(J). \tag{9}$$

Forms of Eqs. (5)–(7) look the same as those of Eqs. (1, 4, 3), indicate that Eqs. (1, 4, 3) satisfy the coordinate-transformation invariant theory.

Then, we can further introduce the specific coordinate transformation:

$$r' = \left(\frac{R_2 - R_1}{R_2}\right)r + R_1, \theta' = \theta, z' = z. \tag{10}$$

Namely, one point in the virtual space expands to a cylinder in the physical space ($r\leqslant R_1$), while the area beyond the outer circumference of the annulus ($r > R_2$) remains intact [Fig. 1(a)]. The key concept lies in that the thermal flow in a virtual space is compressed into a predetermined physical space by means of both an anisotropic viscosity tensor and an anisotropic thermal conductivity tensor. According to derivations in Appendix A.2, we can obtain two transformed parameters of the 2$D$ ideal cloak as

$$\mu' = \begin{pmatrix}\mu'_{rr} & \mu'_{r\theta}\\ \mu'_{\theta r} & \mu'_{\theta\theta}\end{pmatrix} = \begin{pmatrix}\dfrac{r'}{r'-R_1} & 0\\ 0 & \dfrac{r'-R_1}{r'}\end{pmatrix}\mu$$
$$k' = \begin{pmatrix}k'_{rr} & k'_{r\theta}\\ k'_{\theta r} & k'_{\theta\theta}\end{pmatrix} = \begin{pmatrix}\dfrac{r'-R_1}{r'} & 0\\ 0 & \dfrac{r'}{r'-R_1}\end{pmatrix}k \quad , R_1\leqslant r'\leqslant R_2. \tag{11}$$

It should be mentioned that $\mu'$ and $k'$ denote the effective viscosity and the effective conductivity, respectively. According to effective medium theory [26,50,52], these effective values can be fabricated by metamaterials.

However, because values of $\mu'$ and $k'$ will equal infinity or zero (singularity) at $r' = R_1$ and vary sharply from $R_1$ to $R_2$, it is difficult for experimentalist to design and fabricate $\mu'$ and $k'$. Instead of parameters for ideal cloaks, a reduced set of material parameters has been considered to tackle this type of problems in the electromagnetics cloak [6], acoustic cloak [13], thermal-conductive cloak [26] and hydrodynamic cloak [50], respectively. Likewise, we can also calculate the mitigated transformed viscosity tensor ($\mu''$) and the mitigated transformed thermal conductivity tensor ($k''$) as follows, respectively.

$$\mu'' = \begin{pmatrix}\mu''_{rr} & \mu''_{r\theta}\\ \mu''_{\theta r} & \mu''_{\theta\theta}\end{pmatrix} = n\begin{pmatrix}\left(\dfrac{R_2-R_1}{R_2}\right)^2\left(\dfrac{r'}{r-R_1}\right)^2 & 0\\ 0 & \left(\dfrac{R_2-R_1}{R_2}\right)^2\end{pmatrix}\mu$$
$$k'' = \begin{pmatrix}k''_{rr} & k''_{r\theta}\\ k''_{\theta r} & k''_{\theta\theta}\end{pmatrix} = \frac{1}{n}\begin{pmatrix}\left(\dfrac{R_2}{R_2-R_1}\right)^2\left(\dfrac{r'-R_1}{r'}\right)^2 & 0\\ 0 & \left(\dfrac{R_2}{R_2-R_1}\right)^2\end{pmatrix}k, \tag{12}$$

where $R_1\leqslant r'\leqslant R_2, n$ denotes a compensation factor and equals 1.5. Herein, due to variations of $\mu''$ and $k''$ exclusively in the radial axis, this approach may significantly reduce experimental difficulties.

According to Eqs. (11,12), the proposed thermo-hydrodynamic cloak regresses to a thermal-conductive cloak [24,26] in the absence of the convection and to a hydrodynamic cloak [50] in the absence of the heat transfer, suggesting that the proposed study integrates both the thermal conductive cloak and the hydrodynamic counterpart.

## 3. Computational simulations

With Eqs. (1)–(3) and Eqs. 11,12, computational simulations are conducted to demonstrate the validity of the thermo-hydrodynamic cloak using user-defined Coefficient Form PDE (partial differential equations) interface in COMSOL Multiphysics, a commercial finite-element package.

Consider a horizontally-situated cylindrical object impermeable to the fluid (regime III in Fig. 1(b)) surrounded by a concentric metamaterial shell (regime II). This system is immersed in a background fluid flow (regime I) subject to top and bottom Dirichlet boundary conditions, with $\triangle T = 20$ K ($T_2 > T_1$) and an inlet velocity predetermined by $\triangle p = 3$ Pa ($p_2 > p_1$) in the y direction, as well as subject to two insulated nonslip sidewalls. $H\times W\times D$ denotes height × width × depth of the computational domain, where $D$ denotes the depth in z direction with $D\ll W$ and $H$. Because of $D\ll W$ and $H$, the proposed flow, known as Hele-Shaw flow [53,54], can be treated as a two-dimensional one (Fig. 1

**Table A1**
Thermal properties of the object and the background at room temperature 293.15 K and geometry scales.

| | $c_p$[J/(kg·K)] | $\rho$[kg/m$^3$] | $\mu$[Pa·s] | $k$[W/(m·K)] |
|---|---|---|---|---|
| Object (copper) | 385 | 8933 | N/A | 401 |
| Background (water) | 4179 | 997.1 | $10^{-3}$ | 0.613 |
| Geometry scales | $R_1 = 2$ mm | $R_2 = 4$ mm | $H = W =$ 1 cm | $D = 50$ μm |

(b)). For clarity, thermal properties of the object and the background at room temperature 293.15 K and geometry scales are presented in Table A1 (See Appendix).

Fig. 2(a, e) present velocity and temperature fields of the background case with no object perturbations in the domain. Due to the absence of perturbations in the system, streamlines (black color) and isobars (white color) perpendicularly intersect and remain uniform. Owing to the heat convection effect and the prescription of Dirichlet temperature boundary condition at the top of the system, temperature contours show nonuniformity and aggregate near the top wall. However, when an object is placed in the fluid, streamlines, isobars and isotherms near the surface tend to be distorted [Fig. 2(b, f)].

In Fig. 2(c, g), because both the incoming fluid flow and the incoming convective heat flux that are supposed to impinge on the object cannot penetrate into the object nor can they enter the background, they are channeled into the cloak. These rapid detours remove the disturbance of velocity and temperature fields and create straight

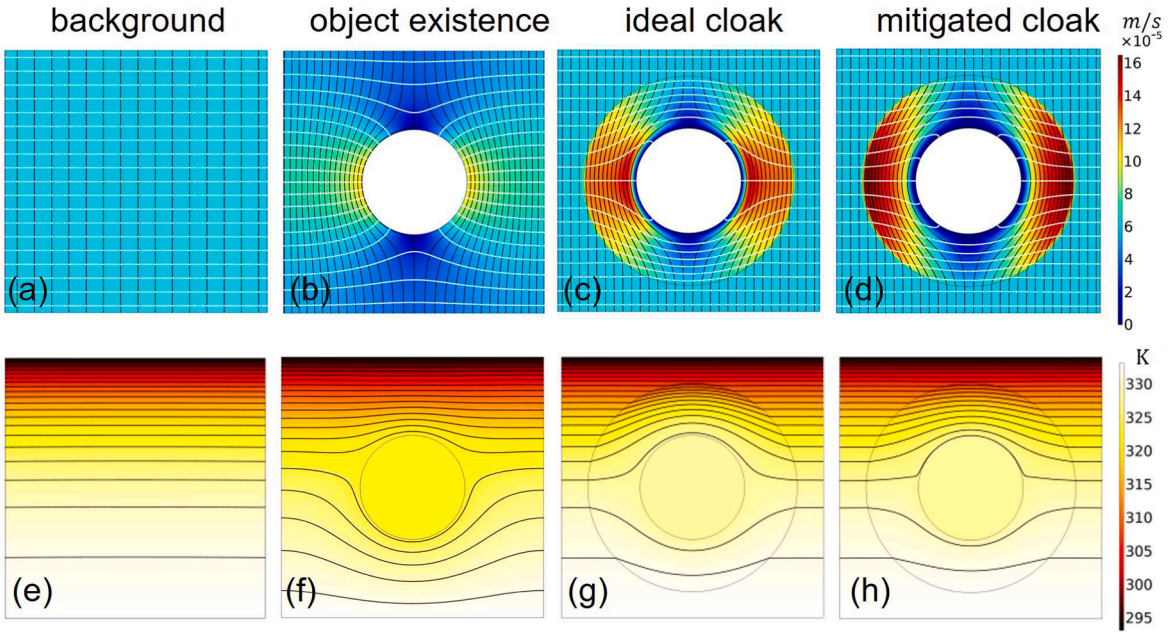


**Fig. 2.** Velocity and temperature distributions for uniform fields. (a - d) Velocity profiles superimposed with streamlines (black color) and isobars (white color). (e - h) Temperature profiles superimposed with isotherms (black color).

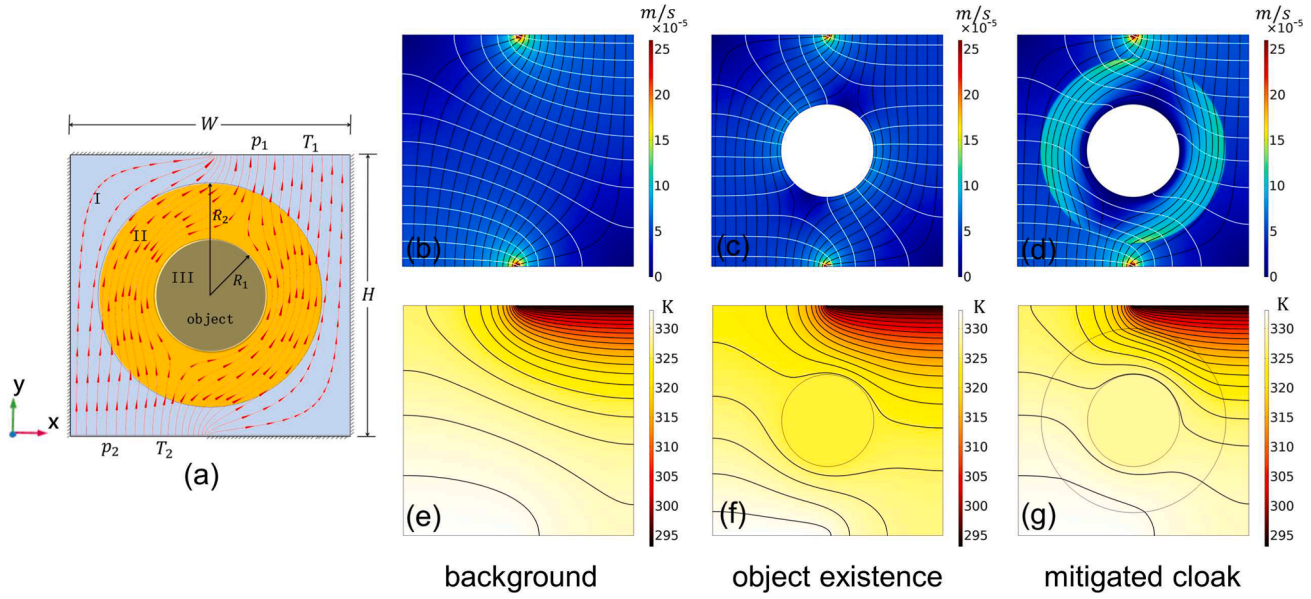


**Fig. 3.** Velocity and temperature distributions for non-uniform fields. (a) Schematic model. (b - d) Velocity profiles superimposed with streamlines (black color) and isobars (white color). (e - g) Temperature profiles superimposed with isotherms (black color).

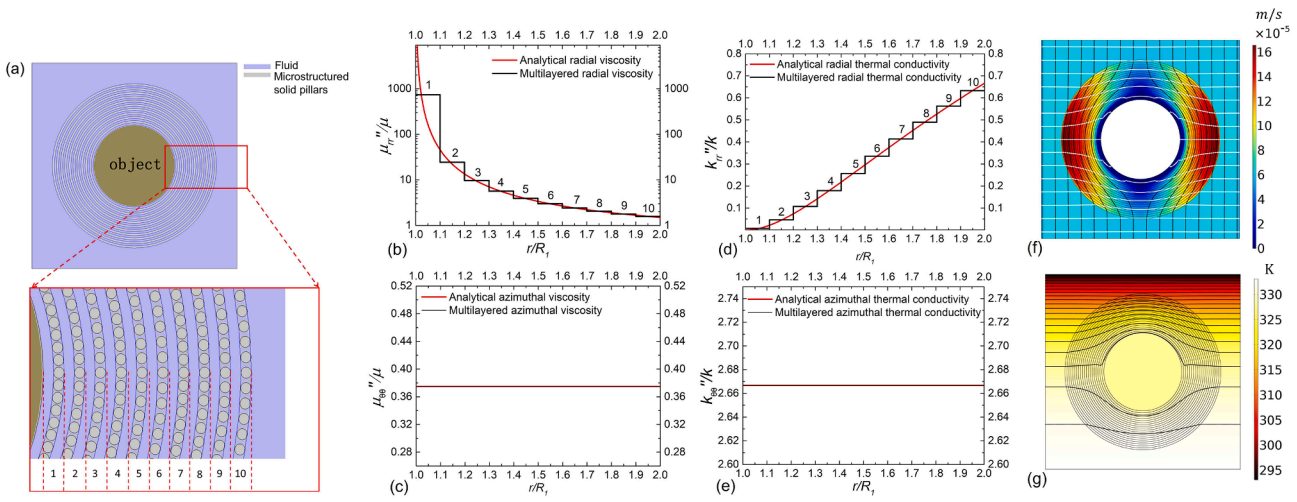


**Fig. 4.** Experimental fabrications of the thermo-hydrodynamic metamaterial cloak. (a) Schematic diagram of ten-layered fluid-micropillar alternating structure of the multilayered cloak. (b - c) Discretized viscosity tensor in each layer along radial (upside) and azimuthal (downside) axes. (d - e) Discretized thermal conductivity tensor in each layer along radial (upside) and azimuthal (downside) axes. (f) Velocity profiles superimposed with streamlines (black color) and isobars (white color) for the multilayered cloak. (g) Temperature profiles superimposed with isotherms (black color) for the multilayered cloak.

streamlines and temperature contours outside the cloak, resulting in the equality of velocity and temperature fields outside the cloak to those in the background. Because an outside observer is unaware of the presence of the object, these phenomena imply that the object immersed in the flow can be hidden both thermally and hydrodynamically.

Likewise, as the object is encircled with the mitigated thermo-hydrodynamic cloak, velocity and temperature fields appear similar to those of the ideal cloak with straight streamlines and temperature contours [Fig. 2(d, h)]. In addition, because the tangential component $\mu''_{\theta\theta}$ of the mitigated thermo-hydrodynamic cloak near the object surface surpasses that of the ideal thermo-hydrodynamic cloak, the hydrodynamic boundary layer of the mitigated thermo-hydrodynamic cloak thickens in comparison with the ideal thermo-hydrodynamic cloak.

To further quantitatively check the validity of the mitigated thermo-hydrodynamic cloak, we present velocity distributions versus $x/R_2$ at $y = 0, -H/4$, and $-9H/20$ [Fig. A1(a) in Appendix], as well as temperature distributions versus $y/R_2$ at $x = 0, H/4$, and $9H/20$ [Fig. A1(b) in Appendix]. Then velocity and temperature distributions outside the cloak appear uniform in accordance with those in the background case (magenta dash line), confirming that they are unaffected by the presence of the object.

Furthermore, to check the validity of our proposed cloak under arbitrary boundary conditions, we let the system [Fig. 3(a)] immerse in a background fluid flow subject to the bottom-left half and the top-right half Dirichlet boundary conditions, with $\triangle T = 20$ K ($T_2 > T_1$) and an inlet velocity predetermined by $\triangle p = 3$ Pa ($p_2 > p_1$) on the bottom-left half and the top-right half walls. On remaining walls of the system nonslip and insulated boundary conditions are imposed.

Likewise, no perturbations due to the presence of the object in velocity and temperature fields of the background case take place in Fig. 3 (b, e). When an object is placed in the fluid, streamlines, isobars and isotherms near the surface tend to be disturbed [Fig. 3(c, f)]. As the object is encircled with the mitigated cloak [Fig. 3(d, g)], velocity and temperature distributions outside the cloak appear uniform in accordance with those in the background case [Fig. 3(b, e)], confirming that they are unaffected by the presence of the object under non-uniform fields.

To further quantitatively check the validity of the mitigated thermo-hydrodynamic cloak under non-uniform boundary conditions, we also present velocity distributions versus $x/R_2$ at $y = 0, -H/4$, and $-9H/20$ [Fig. A2(a) in Appendix], as well as temperature distributions versus $y/R_2$ at $x = 0, H/4$, and $9H/20$ [Fig. A2(b) in Appendix]. We can observe that velocity and temperature distributions outside the cloak at different positions differ from one another, but that they coincide with those in the background case (dashed line), confirming that they are unaffected by the presence of the object [Fig. A2].

Because the viscosity and the thermal conductivity must behave as tensors, they cannot be naturally obtained from traditional materials. To fabricate the thermo-hydrodynamic cloak realistically, researchers can use multilayered fluid-micropillar alternating structure [Fig. 4(a)] based on the effective medium theory [6,24,26,50,55,56]. In the proposed study, the cloak ($R_1 \leqslant r \leqslant R_2$) are divided into ten annular layers. Then averaged viscosity components of the viscosity tensor [Fig. 4(b-c)] and averaged thermal conductivity components of the thermal conductivity tensor [Fig. 4(d-e)] can be designated to each layer Appendix A.3. Radial viscosity distributions and radial thermal conductivity distributions in the cloak become discretized in a step-like manner (Values also shown in Table A2 of Appendix). According to the report on hydrodynamic metamaterials [50,52], the viscous flow can be manipulated by designing anisotropic micropillars. Expectedly, micropillars can produce different flow velocities in each axis on layers, and this manipulation will equivalently lead to the spatially changing anisotropic viscosity. Namely $\mu_{eff} = \left(\langle \boldsymbol{u}_0 \rangle_s / \langle \boldsymbol{u}_{\text{pillar}} \rangle_s\right) \cdot \mu$, where $\boldsymbol{u}_{\text{pillar}}$ and $\boldsymbol{u}_0$ denote the velocity fields with and without a micropillar, respectively, $\langle \cdot \rangle_s$ stands for the superficially averaged quantity, and $\mu$ denotes the intrinsic viscosity of the fluid. Detailed methods to obtain viscosity tensors fabricated by the fluid-micropillar structure can be found in Ref. [50]. Similarly, because the thermal conductivity tensor consists of the thermal conductivity of fluid and that of micropillars, the anisotropic thermal conductivity can

**Table A2**
Ten-layered viscosity values and thermal conductivity values along the radial axis in Fig. 4(b, d).

| Layer numbers | 1 | 2 | 3 | 4 | 5 | 6 | 7 | 8 | 9 | 10 |
|---|---|---|---|---|---|---|---|---|---|---|
| $\mu''_{rr}/\mu$ | 735.32 | 24.32 | 9.67 | 5.66 | 3.92 | 2.99 | 2.42 | 2.05 | 1.78 | 1.58 |
| $k''_{rr}/k$ | 0.0077 | 0.046 | 0.107 | 0.179 | 0.257 | 0.336 | 0.414 | 0.490 | 0.563 | 0.633 |

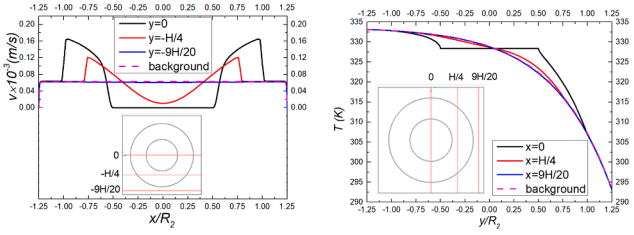


(a) (b)

**Fig. A1.** (a) Velocity distributions versus $x/R_2$ for the mitigated-cloak case at $y = 0$, $-H/4$, and $-9H/20$. (b) Temperature distributions versus $y/R_2$ for the mitigated-cloak case at $x = 0, H/4$, and $9H/20$. Velocity and temperature distributions for the background case with the magenta dashed line are chosen as the reference. (For interpretation of the references to color in this figure legend, the reader is referred to the web version of this article.)

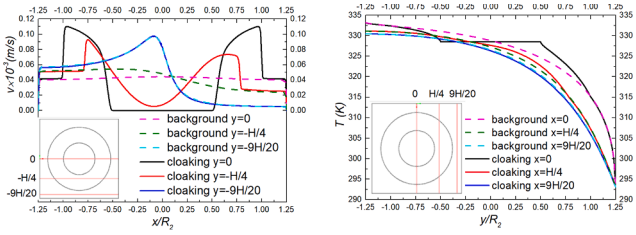


(a) (b)

**Fig. A2.** (a) Velocity distributions versus $x/R_2$ for the mitigated-cloak case under non-uniform boundary conditions at $y = 0$, $-H/4$, and $-9H/20$. (b) Temperature distributions versus $y/R_2$ for the mitigated cloak case at $x = 0$, $H/4$, and $9H/20$. The velocity distribution and the temperature distribution for the background case with dashed lines are chosen as the reference.

be fabricated by manipulating the latter. Namely $k_{eff} = k_{pillar}(1-\phi) + \phi k_f$, subscripts "pillar" and "f" denote solid pillar and fluid, as well as "$\phi$" stands for the volume fraction of fluid. Velocity and temperature distributions outside the multilayered cloak [Fig. 4(f, g)] appear uniform in agreement with those outside the analytical cloak [Fig. 2(d) and (h)] although a slight non-uniformity of isobars is observed at the interface of layers.

As explained above, Figs. 1–3 have demonstrated that the validity of our proposed cloak is unaffected by boundary conditions. Experimental suggestions also have been proposed to show the feasibility of our design in Fig. 4.

## 4. Conclusions

Coupling hydrodynamics and the energy transport, we have established transformation heat transfer for fabricating thermal metamaterials. This establishment has lifted previous limitations imposed in problems of thermal conduction, porous media, and pure hydrodynamics. Based on transformation heat transfer, we have analytically and numerically demonstrated that thermo-hydrodynamic cloaks can manipulate heat fluxes and convective flows simultaneously for creeping flows. Our investigation may lay the foundation for future research in areas of thermo-hydrodynamic metamaterials, such as thermo-hydrodynamic concentrators, thermo-hydrodynamic rotators, and thermo-hydrodynamic illusions/camouflages among others. Besides, it also facilitates the realization of experiments as well as helps researchers identify characteristic flow and thermal parameters.

## CRediT authorship contribution statement

**Bin Wang:** Conceptualization, Methodology, Investigation, Software, Validation, Data curation, Visualization, Writing - original draft, Writing - review & editing, Funding acquisition. **Tien-Mo Shih:** Writing - original draft, Writing - review & editing, Supervision. **Jiping Huang:** Writing - original draft, Writing - review & editing, Supervision, Funding acquisition.

## Declaration of Competing Interest

The authors declare that they have no known competing financial interests or personal relationships that could have appeared to influence the work reported in this paper.

## Acknowledgments

This work is funded by the China Postdoctoral Science Foundation under Grant No. 2019M661354, by the National Natural Science Foundation of China under Grants No. 11725521 and No. 12035004, and by the Science and Technology Commission of Shanghai Municipality under Grant No. 20JC1414700.

## Appendix A

### A.1. Transformation heat-transfer equations

For incompressible flows at steady state, the governing equations can be written as

$$\nabla\cdot\boldsymbol{u} = 0 \tag{A1}$$

$$\nabla p = \mu\nabla^2\boldsymbol{u} \tag{A2}$$

$$\rho c_p\nabla\cdot(\boldsymbol{u}T) = \nabla\cdot(k\nabla T) \tag{A3}$$

Since $\nabla\times(\nabla\times\boldsymbol{u}) = \nabla(\nabla\cdot\boldsymbol{u}) - \nabla^2\boldsymbol{u}$ and Eq. (A1), we can obtain

$$\nabla^2\boldsymbol{u} = -\nabla\times(\nabla\times\boldsymbol{u}).$$

We take divergence $(\nabla\cdot)$ on two sides of above equation.

$$\nabla\cdot\nabla^2\boldsymbol{u} = -\nabla\cdot[\nabla\times(\nabla\times\boldsymbol{u})] = 0.$$

Therefore, Eq. (A2) can be transformed into Pressure-Laplace equation

$$\nabla\cdot(\mu^{-1}\nabla p) = 0. \tag{A4}$$

According to the previous work [24], the heat conduction equation can maintain invariant under coordinate transformation. Therefore, we can introduce a Jacobian transformation matrix ($J$), the equation from virtual space $\boldsymbol{x}(x,y,z)$ to physical space $\boldsymbol{x}'(x',y',z')$ would keep invariant:

$$\nabla'\cdot\left(\frac{J\mu^{-1}J^{\mathrm{T}}}{\det(J)}\nabla' p'\right)=0. \tag{A5}$$

Then we can introduce $\mu'^{-1}=J\mu^{-1}J^{\mathrm{T}}/\det(J)$. Namely,

$$\mu'=\det(J)\cdot J^{-1}\mu J^{-\mathrm{T}}. \tag{A6}$$

Hence, Eq. (A5) can be written as

$$\nabla'\cdot\left(\mu'^{-1}\nabla' p'\right)=0, \tag{A7}$$

Eq. (A7) maintains the same form with Eq. (A4).

Meanwhile, for Eq. (A3), we also have

$$\rho c_p\nabla'\cdot\left(\frac{J\boldsymbol{u}}{\det(J)}T'\right)=\nabla'\cdot\left(\frac{JkJ^{\mathrm{T}}}{\det(J)}\nabla' T'\right), \tag{A8}$$

we can obtain

$$\rho c_p\nabla'\cdot(\boldsymbol{u}'T')=\nabla'\cdot(k'\nabla' T'), \tag{A9}$$

where $\boldsymbol{u}'=J\boldsymbol{u}/\det(J)$ and

$$k'=JkJ^{\mathrm{T}}/\det(J). \tag{A10}$$

Equation. (A9) remains the same form as Eq. (A3). In conclusion, we have proven that Eqs. (A1, A3, A4) remain invariant under coordinate transformation.

### *A.2. Parameters of thermo-hydrodynamic cloaks*

To obtain parameters of thermo-hydrodynamic cloaks, we should obtain the Jacobian transformation matrix ($J$) first. The Jacobian transformation matrix from virtual space $\boldsymbol{x}(x,y,z)$ to physical space $\boldsymbol{x}'(x',y',z')$ is shown as

$$J_{x'x}=\begin{pmatrix}\frac{\partial x'}{\partial x} & \frac{\partial x'}{\partial y} & \frac{\partial x'}{\partial z}\\ \frac{\partial y'}{\partial x} & \frac{\partial y'}{\partial y} & \frac{\partial y'}{\partial z}\\ \frac{\partial z'}{\partial x} & \frac{\partial z'}{\partial y} & \frac{\partial z'}{\partial z}\end{pmatrix}. \tag{A11}$$

The relation of Jacobian transformation matrix between Cartesian and cylindrical coordinate is expressed by $J_{x'x}=J_{x'r'}J_{r'r}J_{rx}$, namely the transformation process: $\boldsymbol{x}(x,y,z)\rightarrow\boldsymbol{r}(r,\theta,z)\rightarrow\boldsymbol{r}'(r',\theta',z')\rightarrow\boldsymbol{x}'(x',y',z')$, where

$$J_{x'r'} = \begin{pmatrix} \frac{\partial x'}{\partial r'} & \frac{\partial x'}{r'\partial \theta'} & \frac{\partial x'}{\partial z'} \\ \frac{\partial y'}{\partial r'} & \frac{\partial y'}{r'\partial \theta'} & \frac{\partial y'}{\partial z'} \\ \frac{\partial z'}{\partial r'} & \frac{\partial z'}{r'\partial \theta'} & \frac{\partial z'}{\partial z'} \end{pmatrix},$$

$$J_{r'r} = \begin{pmatrix} \frac{\partial r'}{\partial r} & \frac{\partial r'}{r\partial \theta} & \frac{\partial r'}{\partial z} \\ \frac{r'\partial \theta'}{\partial r} & \frac{r'\partial \theta'}{r\partial \theta} & \frac{r'\partial \theta'}{\partial z} \\ \frac{\partial z'}{\partial r} & \frac{\partial z'}{r\partial \theta} & \frac{\partial z'}{\partial z} \end{pmatrix}, \tag{A12}$$

$$J_{rx} = \begin{pmatrix} \frac{\partial r}{\partial x} & \frac{\partial r}{\partial y} & \frac{\partial r}{\partial z} \\ \frac{r\partial \theta}{\partial x} & \frac{r\partial \theta}{\partial y} & \frac{r\partial \theta}{\partial z} \\ \frac{\partial z}{\partial x} & \frac{\partial z}{\partial y} & \frac{\partial z}{\partial z} \end{pmatrix}.$$

For the coordinate transformation,

$$r' = \left(\frac{R_2 - R_1}{R_2}\right) r + R_1, \theta' = \theta, z' = z, \tag{A13}$$

we can obtain the Jacobian transformation matrix ($J_{x'x}$ is simplified as $J$) as

$$\begin{aligned} J &= R(\theta') \begin{pmatrix} \frac{R_2 - R_1}{R_2} & 0 & 0 \\ 0 & \frac{r'}{r} & 0 \\ 0 & 0 & 1 \end{pmatrix} R^{-1}(\theta) \\ &= R(\theta') \begin{pmatrix} \frac{R_2 - R_1}{R_2} & 0 & 0 \\ 0 & \left(\frac{r'}{r' - R_1}\right)\left(\frac{R_2 - R_1}{R_2}\right) & 0 \\ 0 & 0 & 1 \end{pmatrix} R^{-1}(\theta'), \end{aligned} \tag{A14}$$

where

$$R(\theta') = \begin{pmatrix} \cos\theta' & -\sin\theta' & 0 \\ \sin\theta' & \cos\theta' & 0 \\ 0 & 0 & 1 \end{pmatrix}. \tag{A15}$$

Hence, we can achieve

$$\det(J) = \left(\frac{R_2 - R_1}{R_2}\right)^2 \left(\frac{r'}{r' - R_1}\right). \tag{A16}$$

According to Eqs. (A6, A10), we can obtain the transformed dynamic viscosity tensor and the transformed thermal conductivity tensor for the cylindrical cloak under cylindrical coordinate system:

$$\mu' = \begin{pmatrix} \mu'_{rr} & \mu'_{r\theta} & \mu'_{rz} \\ \mu'_{\theta r} & \mu'_{\theta\theta} & \mu'_{\theta z} \\ \mu'_{zr} & \mu'_{z\theta} & \mu'_{zz} \end{pmatrix}$$

$$= \begin{pmatrix} \frac{r'}{r'-R_1} & 0 & 0 \\ 0 & \frac{r'-R_1}{r'} & 0 \\ 0 & 0 & \left(\frac{R_2-R_1}{R_2}\right)^2 \left(\frac{r'}{r'-R_1}\right) \end{pmatrix} \mu, \tag{A17}$$

$$k' = \begin{pmatrix} k'_{rr} & k'_{r\theta} & k'_{rz} \\ k'_{\theta r} & k'_{\theta\theta} & k'_{\theta z} \\ k'_{zr} & k'_{z\theta} & k'_{zz} \end{pmatrix}$$

$$= \begin{pmatrix} \frac{r'-R_1}{r'} & 0 & 0 \\ 0 & \frac{r'}{r'-R_1} & 0 \\ 0 & 0 & \left(\frac{R_2}{R_2-R_1}\right)^2 \left(\frac{r'-R_1}{r'}\right) \end{pmatrix} k. \tag{A18}$$

Similarly to the treatment that reduces 3*D* flows into 2*D* ones [50], the dynamic viscosity tensor and the thermal conductivity tensor can be reduced as

$$\mu' = \begin{pmatrix} \mu'_{rr} & \mu'_{r\theta} \\ \mu'_{\theta r} & \mu'_{\theta\theta} \end{pmatrix} = \begin{pmatrix} \frac{r'}{r'-R_1} & 0 \\ 0 & \frac{r'-R_1}{r'} \end{pmatrix} \mu$$

$$k' = \begin{pmatrix} k'_{rr} & k'_{r\theta} \\ k'_{\theta r} & k'_{\theta\theta} \end{pmatrix} = \begin{pmatrix} \frac{r'-R_1}{r'} & 0 \\ 0 & \frac{r'}{r'-R_1} \end{pmatrix} k \quad , R_1 \leqslant r' \leqslant R_2. \tag{A19}$$

### *A.3. Ten-layered viscosity values and thermal conductivity values along the radial axis*

Averaged values of viscosity and thermal conductivity, shown in Fig. 4(b-e) in black, are obtained by mean-value theorems for definite integrals based on red lines in Fig. 4(b-e). Due to the narrowness of each layer, we can calculate each layer by mean-value theorems for definite integrals below:

$$\mu_n = \frac{10}{(R_2-R_1)} \int_{R_1+r_n}^{R_1+r_{n+1}} \frac{\mu''_{rr}}{\mu} dr, \tag{A20}$$

$$k_n = \frac{10}{(R_2-R_1)} \int_{R_1+r_n}^{R_1+r_{n+1}} \frac{k''_{rr}}{k} dr, \tag{A21}$$

where $r_n = \frac{n-1}{10}(R_2-R_1), n = 1,2,3,\ldots,8,9,10.$

Therefore, we can obtain ten-layered viscosity values and thermal conductivity values in Table A2.

## References


[1] U. Leonhardt, Optical conformal mapping, Science 312 (5781) (2006) 1777–1780.
[2] V.M. Shalaev, Transforming light, Science 322 (5900) (2008) 384–386.
[3] A. Alu, N. Engheta, Multifrequency optical invisibility cloak with layered plasmonic shells, Phys. Rev. Lett. 100 (11) (2008) 113901.
[4] H. Chen, C.T. Chan, P. Sheng, Transformation optics and metamaterials, Nat. Mater. 9 (5) (2010) 387.
[5] J.B. Pendry, D. Schurig, D.R. Smith, Controlling electromagnetic fields, Science 312 (1780–1782) (2006) 5781.

[6] D. Schurig, J. Mock, B. Justice, S.A. Cummer, J.B. Pendry, A. Starr, D.R. Smith, Metamaterial electromagnetic cloak at microwave frequencies, Science 314 (5801) (2006) 977–980.
[7] A. Greenleaf, Y. Kurylev, M. Lassas, U. Leonhardt, G. Uhlmann, Cloaked electromagnetic, acoustic, and quantum amplifiers via transformation optics, Proc. Nat. Acad. Sci. 109 (26) (2012) 10169–10174.
[8] F. Gömöry, M. Solovyov, J. Šouc, C. Navau, J. Prat-Camps, A. Sanchez, Experimental realization of a magnetic cloak, Science 335 (6075) (2012) 1466–1468.
[9] J. Zhu, W. Jiang, Y. Liu, G. Yin, J. Yuan, S. He, Y. Ma, Three-dimensional magnetic cloak working from dc to 250 khz, Nat. Commun. 6 (2015) 8931.
[10] H. Chen, C. Chan, Acoustic cloaking in three dimensions using acoustic metamaterials, Appl. Phys. Lett. 91 (18) (2007) 183518.
[11] L. Zigoneanu, B.-I. Popa, S.A. Cummer, Three-dimensional broadband omnidirectional acoustic ground cloak, Nat. Mater. 13 (4) (2014) 352.
[12] M. Farhat, S. Enoch, S. Guenneau, A. Movchan, Broadband cylindrical acoustic cloak for linear surface waves in a fluid, Phys. Rev. Lett. 101 (13) (2008) 134501.
[13] S. Zhang, C. Xia, N. Fang, Broadband acoustic cloak for ultrasound waves, Phys. Rev. Lett. 106 (2) (2011) 024301.
[14] S. Zou, Y. Xu, R. Zatianina, C. Li, X. Liang, L. Zhu, Y. Zhang, G. Liu, Q.H. Liu, H. Chen, et al., Broadband waveguide cloak for water waves, Phys. Rev. Lett. 123 (7) (2019) 074501.
[15] S. Zhang, D.A. Genov, C. Sun, X. Zhang, Cloaking of matter waves, Phys. Rev. Lett. 100 (12) (2008) 123002.
[16] A. Greenleaf, Y. Kurylev, M. Lassas, G. Uhlmann, Approximate quantum cloaking and almost-trapped states, Phys. Rev. Lett. 101 (22) (2008) 220404.
[17] S.B. Riffat, X. Ma, Thermoelectrics: a review of present and potential applications, Appl. Therm. Eng. 23 (8) (2003) 913–935.
[18] C. An, J. Su, Improved lumped models for transient combined convective and radiative cooling of multi-layer composite slabs, Appl. Therm. Eng. 31 (14–15) (2011) 2508–2517.
[19] X. Yin, Q. Chen, N. Pan, Feasibility of perspiration based infrared camouflage, Appl. Therm. Eng. 36 (1) (2012) 32–38.
[20] J. Allison, K. Bell, J.A. Clarke, A. Cowie, A. Elsayed, G. Flett, G. Oluleye, A. Hawkes, G. Hawker, N. Kelly, et al., Assessing domestic heat storage requirements for energy flexibility over varying timescales, Appl. Therm. Eng. 136 (2018) 602–616.
[21] J. Hyun, S. Wang, Systematically engineered thermal metastructure for rapid heat dissipation/diffusion by considering the thermal eigenvalue, Appl. Therm. Eng. 157 (2019) 113487.
[22] C. Fan, Y. Gao, J. Huang, Shaped graded materials with an apparent negative thermal conductivity, Appl. Phys. Lett. 92 (25) (2008) 251907.
[23] T. Chen, C.-N. Weng, J.-S. Chen, Cloak for curvilinearly anisotropic media in conduction, Appl. Phys. Lett. 93 (11) (2008) 114103.
[24] S. Guenneau, C. Amra, D. Veynante, Transformation thermodynamics: cloaking and concentrating heat flux, Opt. Express 20 (7) (2012) 8207–8218.
[25] S. Narayana, Y. Sato, Heat flux manipulation with engineered thermal materials, Phys. Rev. Lett. 108 (21) (2012) 214303.
[26] R. Schittny, M. Kadic, S. Guenneau, M. Wegener, Experiments on transformation thermodynamics: molding the flow of heat, Phys. Rev. Lett. 110 (19) (2013) 195901.
[27] Y. Ma, Y. Liu, M. Raza, Y. Wang, S. He, Experimental demonstration of a multiphysics cloak: manipulating heat flux and electric current simultaneously, Phys. Rev. Lett. 113 (20) (2014) 205501.
[28] Y. Li, X. Shen, Z. Wu, J. Huang, Y. Chen, Y. Ni, J. Huang, Temperature-dependent transformation thermotics: From switchable thermal cloaks to macroscopic thermal diodes, Phys. Rev. Lett. 115 (19) (2015) 195503.
[29] Y. Li, X. Bai, T. Yang, H. Luo, C.-W. Qiu, Structured thermal surface for radiative camouflage, Nat. Commun. 9 (1) (2018) 273.
[30] T. Han, X. Bai, D. Gao, J.T. Thong, B. Li, C.-W. Qiu, Experimental demonstration of a bilayer thermal cloak, Phys. Rev. Lett. 112 (5) (2014) 054302.
[31] H. Xu, X. Shi, F. Gao, H. Sun, B. Zhang, Ultrathin three-dimensional thermal cloak, Phys. Rev. Lett. 112 (5) (2014) 054301.
[32] Y. Li, K.-J. Zhu, Y.-G. Peng, W. Li, T. Yang, H.-X. Xu, H. Chen, X.-F. Zhu, S. Fan, C.-W. Qiu, Thermal meta-device in analogue of zero-index photonics, Nat. Mater. 18 (1) (2019) 48.
[33] T. Han, X. Bai, J.T.L. Thong, B. Li, C. Qiu, Full control and manipulation of heat signatures: Cloaking, camouflage and thermal metamaterials, Adv. Mater. 26 (11) (2014) 1731–1734.
[34] T. Yang, X. Bai, D. Gao, L. Wu, B. Li, J.T.L. Thong, C. Qiu, Invisible sensors: Simultaneous sensing and camouflaging in multiphysical fields, Adv. Mater. 27 (47) (2015) 7752–7758.
[35] R. Hu, S. Zhou, Y. Li, D.-Y. Lei, X. Luo, C.-W. Qiu, Illusion thermotics, Adv. Mater. 30 (22) (2018) 1707237.
[36] G. Wehmeyer, T. Yabuki, C. Monachon, J. Wu, C. Dames, Thermal diodes, regulators, and switches: Physical mechanisms and potential applications, Appl. Phys. Rev. 4 (4) (2017) 041304.
[37] X. He, L. Wu, Thermal transparency with the concept of neutral inclusion, Phys. Rev. E 88 (3) (2013) 033201.
[38] L. Xu, S. Yang, J. Huang, Thermal transparency induced by periodic interparticle interaction, Phys. Rev. Appl. 11 (3) (2019) 034056.
[39] M. Raza, Y. Liu, E.H. Lee, Y. Ma, Transformation thermodynamics and heat cloaking: a review, J. Opt. 18 (4) (2016) 044002.
[40] S.R. Sklan, B. Li, Thermal metamaterials: functions and prospects, Natl. Sci. Rev. 5 (2) (2018) 138–141.
[41] I. Peralta, V.D. Fachinotti, J.C.A. Hostos, A brief review on thermal metamaterials for cloaking and heat flux manipulation, Adv. Eng. Mater. 22 (2) (2020) 1901034.
[42] J.-P. Huang, Theoretical Thermotics: Transformation Thermotics and Extended Theories for Thermal Metamaterials, Springer, 2020.
[43] P.T. Bowen, D.R. Smith, Y.A. Urzhumov, Wake control with permeable multilayer structures: The spherical symmetry case, Phys. Rev. E 92 (6) (2015) 063030.
[44] D.R. Culver, E. Dowell, D. Smith, Y. Urzhumov, A. Varghese, A volumetric approach to wake reduction: Design, optimization, and experimental verification, J. Fluids (2016).
[45] Y.A. Urzhumov, D.R. Smith, Fluid flow control with transformation media, Phys. Rev. Lett. 107 (7) (2011) 074501.
[46] Y.A. Urzhumov, D.R. Smith, Flow stabilization with active hydrodynamic cloaks, Phys. Rev. E 86 (5) (2012) 056313.
[47] G. Dai, J. Shang, J. Huang, Theory of transformation thermal convection for creeping flow in porous media: Cloaking, concentrating, and camouflage, Phys. Rev. E 97 (2) (2018) 022129.
[48] G. Dai, J. Huang, A transient regime for transforming thermal convection: Cloaking, concentrating, and rotating creeping flow and heat flux, J. Appl. Phys. 124 (23) (2018) 235103.
[49] W.-S. Yeung, V.-P. Mai, R.-J. Yang, Cloaking: Controlling thermal and hydrodynamic fields simultaneously, Phys. Rev. Appl. 13 (6) (2020) 064030.
[50] J. Park, J.R. Youn, Y.S. Song, Hydrodynamic metamaterial cloak for drag-free flow, Phys. Rev. Lett. 123 (7) (2019) 074502.
[51] F. Tay, Y. Zhang, H. Xu, H. Goh, Y. Luo, B. Zhang, A metamaterial-free fluid-flow cloak, arXiv preprint arXiv: 1908.07169.
[52] K.J. Morton, K. Loutherback, D.W. Inglis, O.K.C. Tsui, J.C. Sturm, S.Y. Chou, R. H. Austin, Hydrodynamic metamaterials: Microfabricated arrays to steer, refract, and focus streams of biomaterials, Proc. Natl. Acad. Sci. USA 105 (21) (2008) 7434–7438.
[53] H.S. Hele-Shaw, The flow of water, Nature 58 (1898) 34.
[54] P.K. Kundu, D.R. Dowling, G. Tryggvason, I.M. Cohen, Fluid mechanics, Academic Press, 2015.
[55] J. Li, Y. Gao, J. Huang, A bifunctional cloak using transformation media, J. Appl. Phys. 108 (7) (2010) 074504.
[56] R. Wang, J. Shang, J. Huang, Design and realization of thermal camouflage with many-particle systems, Int. J. Therm. Sci. 131 (2018) 14–19.